Technical assessment for enhancing environmental sustainability of metallurgical exhaust gases to methanol process via electrochemical energy conversion

Kuo, Po Chih; Özdemir, Faruk; Wu, Yin Ping; Illathukandy, Biju; Wu, Wei; Aziz, Muhammad

DOI
10.1016/j.jclepro.2025.146853

Publication date
2025

Document Version
Final published version

Published in
Journal of Cleaner Production

Citation (APA)
Kuo, P. C., Özdemir, F., Wu, Y. P., Illathukandy, B., Wu, W., & Aziz, M. (2025). Technical assessment for enhancing environmental sustainability of metallurgical exhaust gases to methanol process via electrochemical energy conversion. *Journal of Cleaner Production*, *532*, Article 146853. https://doi.org/10.1016/j.jclepro.2025.146853

Journal of Cleaner Production 532 (2025) 146853

Contents lists available at ScienceDirect

Journal of Cleaner Production

journal homepage: www.elsevier.com/locate/jclepro

Technical assessment for enhancing environmental sustainability of metallurgical exhaust gases to methanol process via electrochemical energy conversion

Po-Chih Kuo [a,*], Faruk Özdemir [b,1], Yin-Ping Wu [c,1], Biju Illathukandy [d,e,1], Wei Wu [c,f,**], Muhammad Aziz [a]

[a] Institute of Industrial Science, The University of Tokyo, 4-6-1 Komaba, Meguro-ku, Tokyo, 153-8505, Japan
[b] Process and Energy Department, Delft University of Technology, Leeghwaterstraat 39, 2628 CB, Delft, the Netherlands
[c] Department of Chemical Engineering, National Cheng Kung University, Tainan, 70101, Taiwan
[d] Centre for Rural Development & Technology, Indian Institute of Technology, Delhi, 110016, India
[e] Department of Mechanical Engineering, Government Engineering College, Kozhikode, Kerala, 673005, India
[f] Academy of Innovative Semiconductor and Sustainable Manufacturing, National Cheng Kung University, Tainan, 70101, Taiwan

HIGHLIGHTS

- A novel process for the valorization of metallurgical gases into methanol is evaluated.
- A trade-off between energy conversion efficiency and carbon reduction potential.
- Process heat demand is the primary contributor to carbon emissions.
- Long-loop gas recirculation configuration offers the lowest carbon intensity of methanol.
- Heat-integration design achieves up to 9 % enhancement in energy conversion efficiency.

ARTICLE INFO

Keywords:
Sustainable ironmaking
CO_2 reduction
Metallurgical gases
Carbon recycling
Renewable methanol
Blast furnace

ABSTRACT

The iron and steel industry is considered as one of the hard-to-abate heavy sectors due to the massive demand for metallurgical coke in the energy-intensive blast furnace (BF) ironmaking process. In this work, an electrochemical conversion of two major metallurgical exhaust gases, namely, blast furnace (BFG) and coke oven gas (COG) into renewable methanol (CH_3OH) is proposed for deeply decarbonizing steel production. An innovative low-carbon BF ironmaking process, which combines solid oxide cells (i.e., renewable-powered co-electrolysis and COG-fed solid oxide fuel cells) and oxyfuel combustion for CO_2 capture, is thermodynamically modeled to evaluate various performance metrics in terms of energy conversion efficiency, product yield, and carbon intensity of renewable methanol. To enhance the process conversion efficiency, four different recycling configurations are designed and compared for efficient tail gas utilization: Scenarios 1 and 4 (co-electrolysis and methanol synthesis via short-loop recirculation) and Scenarios 2 and 3 (co-electrolysis and methanol synthesis via long-loop recirculation). The results indicate that efficient tail gas utilization via long-loop recirculation into the co-electrolysis unit could generate a much higher methanol yield than the short-loop design. Up to 73 % carbon conversion efficiency can be achieved, while 30 % energy conversion efficiency can be attained using long-loop design at a recirculation ratio (RR) of 0.8. Nevertheless, a higher RR operation results in increased energy demand associated with the methanol synthesis process, which in turn leads to higher indirect carbon emissions. Overall, the carbon intensity of methanol ranges from approximately 1.05–1.48kg-CO_2/kg-CH_3OH across the four process configurations under the selected RRs. The long-loop design is likely to offer a reduction in CO_2 emissions of up to 57 % compared to the traditional blast furnace ironmaking process. In particular, a maximum energy conversion efficiency of 38 % can be achieved through heat integration, while net negative CO_2

* Corresponding author. Institute of Industrial Science, The University of Tokyo, 4-6-1 Komaba, Meguro-ku, Tokyo 153-8505, Japan
** Corresponding author. Department of Chemical Engineering, National Cheng Kung University, Tainan, 70101, Taiwan.
E-mail addresses: pckuo@iis.u-tokyo.ac.jp (P.-C. Kuo), weiwu@gs.ncku.edu.tw (W. Wu).
[1] These authors contributed equally to this work.

https://doi.org/10.1016/j.jclepro.2025.146853
Received 27 December 2024; Received in revised form 9 October 2025; Accepted 12 October 2025
Available online 29 October 2025

emissions are achievable based on the evaluated system boundary. The developed process not only has great potential to close the carbon loop between steel makers and chemical producers but also efficiently stores energy in the form of renewable methanol.

Nomenclature

D_P	particle diameter (m)
F	Faraday's constant (96485 C mol^{-1})
$H_{2,consumed}$	consumed amount of H_2 (kmol h^{-1})
$H_{2,equivalent}$	equivalent amount of H_2 (kmol h^{-1})
ΔH	enthalpy change of reaction (J mol^{-1})
ΔG	Gibbs free energy change of reaction (J mol^{-1})
I	current (A)
k_i	kinetic factor of species i (kmol kg_{cat}^{-1} s^{-1} bar^{-1})
K_{pi}	equilibrium constant of species i (−)
K_a, K_b, K_c	adsorption constants (bar^n)
LHV_i	lower heating values of species i (kJ kg^{-1})
$\dot{m}_i$	mass flow rate of species i (kg h^{-1})
$O_{2,required}$	required amount of oxygen (kmol h^{-1})
$O_{2,consumed}$	consumed amount of oxygen (kmol h^{-1})
$O_{2,in}$	amount of oxygen enters the cathode (kmol h^{-1})
p_i	partial pressure of species i (bar)
P_{SOEC}	electric power input to SOEC (kW)
$P_{SOFC,AC}$	AC power output from SOFC (kW)
$P_{SOFC,DC}$	DC power output from SOFC (kW)
Q_{SOEC}	heat duty of SOECs (kW)
r_i	reaction rate of species i (mol kg_{cat}^{-1} s^{-1})
ΔS	entropy change of reaction (J $K^{-1}mol^{-1}$)
T	temperature (K)
U	superficial velocity (m s^{-1})
U_f	fuel utilization factor (−)
U_a	oxygen utilization factor (−)
V_{th}	thermoneutral voltage (V)
V_{cell}	cell voltage (V)
η_{inv}	inverter efficiency (%)
η_{En}	energy conversion efficiency (%)
ε	void fraction (−)
μ	fluid viscosity (Pa s)
ϕ_s	particle shape factor (−)
ρ	fluid density (kg m^{-3})

Abbreviations

AC	alternating current
ASU	air separation unit
AUX	auxiliary unit
BF	blast furnace
BFG	blast furnace gas
BOF	basic oxygen furnace
BOFG	basic oxygen furnace gas
COG	coke oven gas
DC	direct current
DME	dimethyl ether
DRI	direct reduction iron
EAF	electric arc furnace
HBI	hot briquetted iron
HI	heat integration
HRSG	heat recovery steam generator
HM	hot metal
LHHW	Langmuir–Hinshelwood–Hougen–Watson
MTBE	methyl tertiary butyl ether
PCI	pulverized coal injection
PFR	plug flow reactor
PSA	pressure swing adsorption
RAFT	raceway adiabatic flame temperature
RR	recirculation ratio
RWGS	reverse water gas reaction
SN	stoichiometric number
SOCs	solid oxide cells
SOECs	solid oxide electrolysis cells
SOFCs	solid oxide fuel cells
ULCOS	ultra–low CO_2 steelmaking
VPSA	vacuum pressure swing adsorption

1. Introduction

Nowadays, the energy-intensive and environmentally hostile iron and steelmaking sector is responsible for approximately 7–9 % of the total global CO_2 emissions, thereby making it a significant contributor to the greenhouse effect (Marocco et al., 2023). The blast furnace (BF)-basic oxygen furnace (BOF) route stands as a well-established and predominant pathway for producing crude steel worldwide, which accounts for approximately 70–75 % of total production, followed by the electric arc furnace (EAF) steelmaking route (Uribe-Soto et al., 2017; Holappa, 2020; Safarian, 2023). According to the World Steel Association, the average global crude steel production over the last five years has touched 1905 million metric tonnes, which is further expected to approach 2200 million metric tonnes by 2050 (World Steel Association; Collis et al., 2021). In this process, metallurgical coke serves multiple functions as an energy source, a producer of reducing agents, and an essential spacer for enhancing gas permeability within the BF ironmaking system. Consequently, a significant amount of CO_2 is emitted into the atmosphere during the ironmaking process, with approximately 62 % originating from the BF subsystem (including the hot stove), 18.4 % from the coke-making plant, and 19.6 % from the sintering plant (Ariyama and Sato, 2006). On average, the carbon emission intensity of crude steel production ranges from around 1.82 to 1.91 t-CO_2/t-crude steel produced (World Steel Association). Compared to the steelmaking process, the ironmaking process accounts for approximately 70–80 % of the total CO_2 emissions in an integrated iron and steel plant. Therefore, priority should be given to promptly addressing the BF ironmaking process to reduce the overall carbon intensity of crude steel production.

To alleviate this environmental burden and improve the steel productivity, the current focus is targeted on rapidly developing the direct reduction iron (DRI)-EAF route at an industrial scale perspective. In the DRI route, the pre-reduced iron ore can be produced with relatively low-carbon intensity fuels such as methane, H_2-rich gas, and even green H_2 as reducing agents for the shaft furnace (Lipiäinen et al., 2024). When combined with an EAF powered by renewable energy sources, this pathway enables the generation of steel with low-carbon emission intensity. However, despite the promise of the DRI-EAF route for deep decarbonizing the iron and steelmaking industry, economic concerns such as the extended lifespan of BFs, typically exceeding 30 years, and the long-term investment commitments involved suggest that the BF-BOF route will likely continue to dominate approximately 50 % of crude steel production till 2050. (Collis et al., 2021).

As a result, a wide range of decarbonization technologies and

strategies for the blast furnace ironmaking process have been explored over the last two decades. A vast majority of the efforts have been placed on utilizing low-carbon fuels such as H_2-rich gas, bio-syngas as reductant sources, and implementing top-gas recycling BF technology (Bailera, 2023; Hu et al., 2023). Additionally, there have also been initiatives to change the type of feedstock, such as incorporating hot briquetted iron (HBI)/DRI into the burden materials and utilizing a blend of biochar and coke (Safarian, 2023). However, the CO_2 reduction potential of these low-carbon BF ironmaking methods is limited due to various operational constraints, including heat balance of the BF, gas permeability, and the shape of the cohesive zone. Indeed, from a practical BF operation viewpoint, the intricate multi-phase flow phenomena inside the furnace pose many technical challenges for implementing pure hydrogen BF injection at an industrial-scale BF. Consequently, exploring innovative decarbonization pathways without significant retrofitting of the existing integrated steel process is imperative.

In this regard, there has been increasing attention on the valorization of metallurgical gases, including blast furnace gas (BFG), coke oven gas (COG), and basic oxygen furnace gas (BOFG). The focus is to transform these steel mill gases into value-added fuels and chemicals, with the goal of closing the carbon loop between steel and chemical producers. Among these gases, BFG is the highest in quantity, followed by COG and BOFG. Considering their calorific values, COG renders the highest energy content as its constituents are largely comprised of H_2 and CH_4, followed by BOFG with high concentrations of CO and BFG, which contains high amounts of inert N_2 (Lundgren et al., 2013; Uribe-Soto et al., 2017). Typically, they are used as energy sources for power and heat generation, supplying the on-site iron and steelmaking process, such as hot blast stoves, coke ovens, sintering, and on-site power plants, and the excess steel-off gases are usually flared. These result in severe environmental pollution and contribute to considerable CO_2 emissions. Hence, reutilizing carbonaceous metallurgical gases, known as smart carbon usage, offers a significant opportunity to reduce the carbon footprint by avoiding CO_2 emissions throughout the conventional fossil-based chemical and fuel manufacturing chain (Artz et al., 2018; Flores-Granobles et al., 2020; Girod, 2020; Collis et al., 2022; Qian et al., 2024).

In contrast to the higher calorific value of COG and BOFG, the enormous quantity of BFG could be regarded as the preferred feedstock for high-value chemical and fuel production from the viewpoints of economic viability and environmental impact (Collis et al., 2021). Many significant fundamental and pilot-scale R&D projects involved in the so-called Carbon2Chem, led by one of the world-leading steelmakers (ThyssenKrupp), have been referred to and analyzed to evaluate the technical feasibility, economic viability, and environmental sustainability of valorizing BFG into methane (CH_4), methanol (CH_3OH), ammonia (NH_3), urea ($CO(NH_2)_2$), etc. (Schittkowski et al., 2018, 2022; Yildirim et al., 2018). For instance, methanol stands out as a representative and essential chemical that could be derived from BFG (Hauser et al., 2022; Deng and Adams II, 2020; Voβ et al., 2022; Bampaou et al., 2023). It is a critical precursor for various downstream chemical production processes such as methyl tertiary butyl ether (MTBE), dimethyl ether (DME), olefins, formaldehyde, acetic acid, etc. (Ateka et al., 2022). In general, methanol production from coal gasification and steam reforming of natural gas results in unavoidable environmental impacts. Therefore, smartly utilizing carbon from steel mill exhaust gases to produce methanol not only meets the global demand for this versatile chemical but also establishes a sustainable carbon value chain across diverse industrial sectors.

In principle, different carbon conversion strategies can be employed to convert cleaned BFG into methanol (Schittkowski et al., 2018). One approach involves blending BFG with other steel mill gases (i.e., COG and BOFG) and subjecting them to reforming processes to achieve the desired stoichiometric number of the inlet gas stream for methanol synthesis (Deng and Adams II, 2020; Xu et al., 2022; Yang et al., 2023). Alternatively, another method is to separate CO_2 from BFG via various CO_2 capture technologies and then perform direct CO_2 hydrogenation with H_2 (Porter et al., 2022; Gentile et al., 2022). A third option involves directly utilizing BFG with or without other steel mill gases, while the required H_2 source is supplied by water electrolysis (Kim and Han, 2020; Hauser et al., 2022; Bampaou et al., 2022; Qiu et al., 2023). Due to the low H_2 content in BFG, external H_2 addition is required for this scenario. Considering the techno-economic evaluation of the different methanol production pathways, Table 1 reveals that the reforming of COG for supplying required H_2 source in the methanol synthesis exhibits the lowest production cost, whereas the renewable-driven H_2 production involved pathway significantly increases the methanol production cost.

Besides, an innovative electrochemical conversion route via co-electrolysis technology is being considered for the valorization of BFG, known as “Power-to-Gas” technology. Electrifying the iron and steel industry is emerging as a leading approach for future carbon-neutral steel production. Although there is limited knowledge on the co-electrolysis of CO_2 from blast furnace gas (BFG), most research has focused on top-gas recycling BF technology (Dipu et al., 2014; Bailera et al., 2021; Kong et al., 2022; Bailera, 2023; Hu et al., 2023).

To the best of our knowledge, little attention has been given to efficient carbon utilization of steel mill gas through coupling co-electrolysis of CO_2 with methanol synthesis, particularly in the absence of works directly coupling with the BF ironmaking model. Therefore, the objective of this work is to develop an innovative and conceptual process design using electrochemical devices, namely, solid oxide fuel cells (SOFCs) and solid oxide electrolysis cells (SOECs), to convert two major steel mill gases (i.e., BFG and COG) into power and methanol. On the other hand, this work also explores novel perspectives on enhancing the sustainability of the BF ironmaking system via integrating an SOFC-based oxy-fuel combustion system to maximize the carbon source utilization. Various process performance indicators, including methanol yield, carbon conversion efficiency, energy efficiency, and carbon intensity, will be evaluated across different recycling configurations to determine the optimal operating maps for this new process.

2. Process description

A simplified flow diagram of the overall integrated blast furnace (BF) ironmaking-solid oxide cells (SOCs)-methanol production is depicted in Fig. 1. Overall, the integrated plant can be classified into four major subsystems: (1) BF ironmaking with CO_2 capture, (2) SOFC-based oxy-fuel combustion, (3) co-electrolysis (SOEC), and (4) methanol synthesis and purification. In this work, the feeding rate of fuel (i.e., both BFG and

Table 1
A summary of methanol production cost via various conversion pathways using steel-work off-gases as feedstock.

Pathway	H_2 source	Plant capacity (kt-MeOH/y)	Production cost	Reference
I	Reforming of COG/Steam/CO_2	145–184	246–264 USD/t-MeOH	Deng and Adams II (2020)
II	Sorption enhanced water-gas shift reaction of BFG/BOFG	109.5–438	574.1–1037.6 EUR/t-MeOH	Gentile et al. (2022)
II	Water-gas shift reaction of BFG + PSA	188.9	344.61–459.54 GBP/t-MeOH	Porter et al. (2022)
III	Steam methane reforming or electrolysis	78.3–113.3	902–1249 USD/t-MeOH	Kim and Han (2020)
III	Electrolysis via proton exchange membrane	605.5–1217.3	1226–1309 EUR/t-MeOH	Bampaou et al. (2022)

Note: Pathway I: BFG + COG/BOFG, Pathway II: Captured CO_2 from BFG + H_2 source, Pathway III: direct conversion of BFG with/without COG and BOFG + H_2 source.

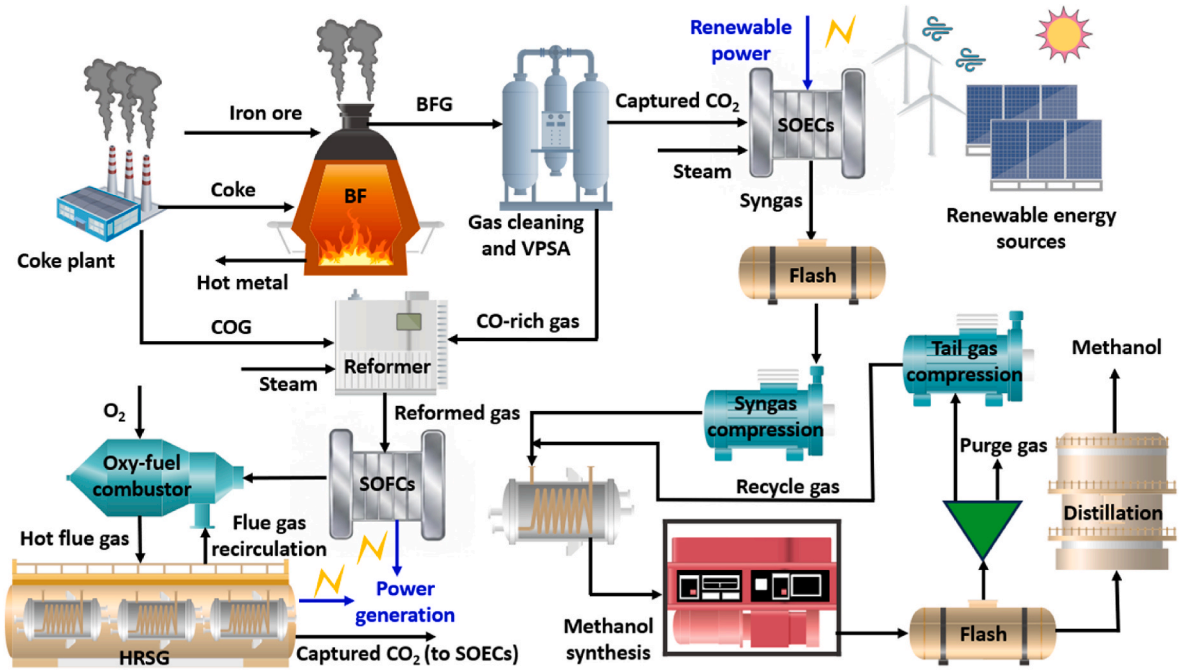

Fig. 1. Schematic of the integrated BF-SOCs-Methanol production process (conceptual illustration).

COG) for methanol and power generation is evaluated based on 1 ton of hot metal (tHM) production from the blast furnace. The generated COG and CO-rich gas separated from the vacuum pressure swing adsorption (VPSA) together feed the oxy-based SOFC + HRSG system for power generation. Approximately 970 kW (DC) or 892 kW (AC) (assuming that a DC-AC inverter conversion efficiency of 92 %) of electricity generated by SOFCs, while approximately 110 kW (AC) generated by HRSG. They can be used to compensate for co-electrolysis SOECs and auxiliary units (i.e., balance of the plant system) in the plant itself.

Based on the above subsystems, four different scenarios with regard to various recycle strategies for tail gas utilization in the integrated BF ironmaking-SOFC-SOEC-methanol synthesis are investigated. The recirculation ratio (RR) is defined as the amount of tail gas being recycled back into the system divided by the total amount of tail gas. The RR is varied over a range from 0.1 to 0.8 in this work. The higher the RR, the more tail gas is recycled into the system. As shown in Fig. 2, the major difference among the four scenarios is the feeding point location of the recycle stream.

In scenario I (S1), both captured CO_2 streams derived from the BF ironmaking system and SOFC-based oxyfuel combustor are mixed with steam and the cathode outlet stream of the co-electrolysis. Subsequently, the mixed stream is sent to the fuel side of the SOEC for syngas production. The required amount of steam in the co-electrolysis unit is calculated by a design spec block according to various RRs to accomplish the desired stoichiometric ratios for methanol synthesis. The initial amount of H_2 is fixed at 10 % (mol%) in the inlet cathode flow via introducing an external H_2 stream (i.e., benchmark case denoted as RR = 0) to avoid the undesired nickel oxidation. Notably, when RR is greater than 0.192, the H_2 concentration at the cathode inlet flow can achieve 10 %, meaning that the external H_2 stream is not necessarily supplied. The discharged syngas from the co-electrolysis unit is subsequently compressed to 70 bar and then fed to the methanol synthesis reactor for methanol production. After passing through a gas-liquid separation unit, the crude methanol is purified in a distillation column. In contrast, the unreacted effluent gas from the flash is regarded as primary carbon emissions from the overall plant.

In scenario II (S2), two recirculation loops are adopted in the integrated system. The first loop is established within the co-electrolysis system, for which the RR is fixed at 0.192, while the second loop is in connection with the tail gas of methanol synthesis with the co-electrolysis unit. In other words, the gas stream from the flash is recycled and mixed with a fresh stream (i.e., containing a CO_2-rich stream, steam, and the mixture of the first recycled stream). Therefore, in S2, only the value of RR in the second recycle loop is changed.

In scenario III (S3), no recycle stream is considered within the co-electrolysis system. Here, the unreacted gas from the methanol synthesis process is recirculated back to the cathode side. In scenario IV (S4), unlike S3, the RR of the first loop is controlled at 0.192, and the effluent

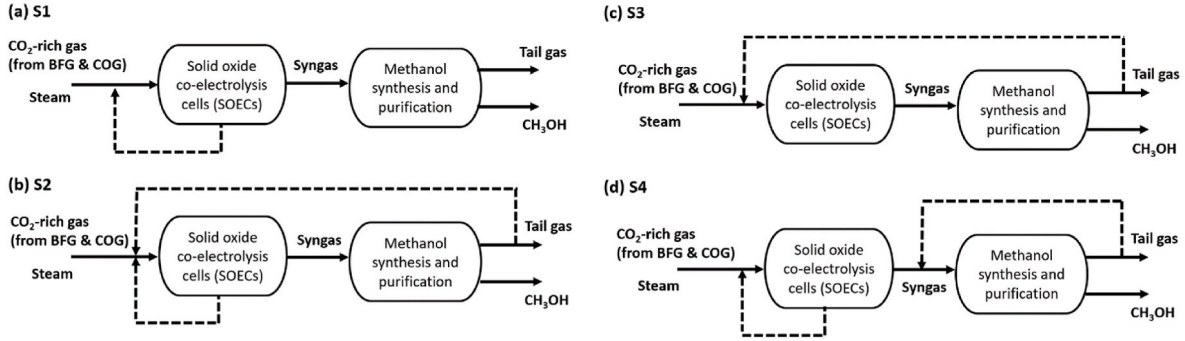

Fig. 2. Four process configurations of the integrated BF-SOCs-Methanol production process.

gas from the methanol synthesis is recirculated to the methanol reactor. Based on the four process configurations, various key performance merits of the integrated BF ironmaking-SOFC-SOEC-methanol synthesis are evaluated and compared comprehensively. On the other hand, the detailed operating conditions for each key subsystem is given in Table 2.

3. Modeling and validation

3.1. Blast furnace model and verification

A thermodynamic modeling approach is used to model the complex chemical reactions that take place in the BF (see Table S1). The developed BF model is established by coupling Aspen Plus® with FactSage software. The lack of metallurgical thermodynamic data in Aspen Plus is overcome by exporting those details from FactSage. This helps to accurately predict the chemical behaviors and product distributions. After setting up the database, a number of Aspen Plus blocks are chosen to represent an industrial-scale BF reactor. In general, the BF can be divided into a series of boundaries, including a heating zone, upper zone, lower zone, and raceway zone (Yilmaz et al., 2017). The schematic of the developed BF is shown in Fig. S1, where ferrous burden materials, coke, and flux first move downwards from the top of the BF, while the hot reducing gas (i.e., CO and H_2) flows upwards from the raceway. In the pre-heating zone, a heat exchanger is used to simulate the heat transfer between the countercurrent solid-gas contact.

In addition, it is assumed that only evaporation of water from solid materials takes place during this stage (Yilmaz et al., 2017), and therefore, two RGibbs reactors (R1 and R2) with restricted equilibrium are employed for this purpose. Another three RGibbs reactors (R3, R4, and R5) are connected in series to model iron ore reduction (i.e., indirect and direct reduction reactions) in the upper and lower furnace zones. In this way, reaction equilibrium calculations based on the Gibbs free energy minimization method are performed. Notably, it is important to specify a suitable boundary equilibrium temperature between each zone. According to the work of Yilmaz et al. (2017), the initial phase equilibrium temperatures of 737, 948, and 1500 °C, corresponding to reactors of R3, R4, and R5, are taken into account to predict the chemical phenomena associated with gas-liquid-solid multi-phase reaction inside the BF. The major chemical reactions considered in the model are summarized in Table S1.

At the lower part of the BF, the hot blast at a temperature of around 1200 °C and a pressure of 4.2 bar along with pulverized coal, is blown into the raceway zone, where, as suggested by Yilmaz et al. (2017), around 60 % of total coke input and pulverized coal are used as a fuel to provide sufficient heat energy for softening and melting the reduced iron. Meanwhile, the hot reducing gas is generated through a series of stepwise reactions, consisting of the devolatilization of coal, oxidation of volatiles and carbon, and carbon solution loss. Based on the thermodynamic data, the theoretical raceway adiabatic flame temperature (RAFT) can be calculated using the last RGibbs reactor model (R6). Eventually, the hot BFG leaves from the top of the BF, whereas the molten hot metal (HM) and molten slag are tapped from the BF by using a separator. It should be noted that the major components of molten slag considered in the present model include CaO, MgO, SiO_2, Al_2O_3, and FeO, while those of BFG mainly contain H_2, CO_2, CO, N_2, and H_2O. In addition, to reflect the realistic operation restrictions of the BF, several simulation constraints with respect to top gas temperature (i.e., 110–150 °C), RAFT (i.e., 2050–2300 °C), CO utilization (i.e., 50–52 %), HM temperature (i.e., ~1500 °C), and basicity of slag (i.e., B_2: 1.10–1.20) are taken into account while solving the mass and energy balance as well as fitting the measured outputs of the BF.

The verification of the developed BF model is conducted by comparing the present results with those obtained from the studies of Suzuki et al. (2015) and Yilmaz et al. (2017). Notably, the volume of BFs considered in the model for the former and latter are 2530 and 5000 m^3, respectively. The key values of the BF model input and output in terms of specific quantities (i.e., per ton of hot metal, tHM) are listed in Table S2 and Table S3. It can be clearly seen that the relative errors between the present model and literature data are almost less than 5 %, with the exception of the H_2 volume fraction in top gas, reflecting that the

Table 2
Operating parameters of main units used in the Aspen Plus simulation.

Sub-systems	Aspen model type	Parameters	Unit	Value
Blast furnace	RStoic, RGibbs	Coke rate	kg/tHM	373.9
		PCI rate	kg/tHM	120
		Hot blast humidity	g/Nm^3	15
		Oxygen Enrichment	%	1.7
		Hot blast temperature	°C	1200
		Hot blast pressure	bar	4.2
		Hot blast rate	Nm^3/tHM	1026.3
		RAFT	°C	2155
		Top gas composition	%	H_2: 3.2 CO_2: 22.8 CO: 21.9 N_2: 52.1
		CO utilization efficiency	%	51
Oxy-fuel-based SOFC	RStoic, RGibbs	Temperature	°C	800
		Pressure	atm	1.2
		Fuel utilization factor	%	85
		DC/AC conversion efficiency	%	92
		Oxygen excess	%	5
		Combustion temperature	°C	1050
		Specific energy consumption for O_2 production	kWh/kg	0.269
Co-electrolysis SOEC	RStoic, RGibbs	Temperature	°C	800
		Pressure	atm	1
		Recirculation ratio	–	0.1–0.8
Methanol synthesis and purification	RPlug, RadFrac	Inlet temperature	°C	225
		Pressure	bar	70
		Stoichiometric ratio	–	2.04–2.05
		Recirculation ratio	–	0.1–0.8
		Reactor length	m	12
		Reactor Diameter	m	0.04
		Reflux ratio	–	2
		Number of stages	–	17

developed BF model is highly reliable in predicting the BF operation and the product distribution (i.e., top gas, liquid pig iron, and molten slag).

3.2. Co-electrolysis model and verification

The SOCs model is developed in co-electrolysis and fuel cell operation. The major electrochemical half-reaction that occurs on cathode and anode electrodes and their overall reaction during the co-electrolysis are shown below:

$$CO_2 + 2e^- \rightarrow CO + O^{2-} \quad (1)$$

$$H_2O + 2e^- \rightarrow H_2 + O^{2-} \quad (2)$$

$$2O^{2-} \rightarrow O_2 + 4e^- \quad (3)$$

$$CO_2 \rightarrow CO + 0.5O_2 \quad (4)$$

$$H_2O \rightarrow H_2 + 0.5O_2 \quad (5)$$

$$H_2O + CO_2 \rightarrow H_2 + CO + O_2 \quad (6)$$

$$CO_2 + H_2 \leftrightarrow CO + H_2O \quad (7)$$

$$CH_4 + H_2O \leftrightarrow CO + 3H_2 \quad (8)$$

The detailed process flowsheet of the SOCs system under co-electrolysis (SOEC) and oxy-fuel combustion-based SOFC operation are plotted in Fig. S2 and S3, respectively.

The co-electrolysis model includes three primary reactors (R1, R2, and R3) to simulate the equilibrium and electrochemical reactions taking place in the electrolyzer stack. At first, the inlet gas stream is fed into the fuel electrode, where the reverse water gas reaction (RWGS) happens at thermodynamic equilibrium modeled by the RGibbs block. Subsequently, the separated CO_2 and steam enter an RStoic block where the relevant electrochemical reactions are represented in this reactor. The produced oxygen flows out with the entrained anode gas, while the remaining mixture of gas gets mixed and passes through another RGibbs block (R3) in which both RWGS (Eq. (7)) and methanation (Eq. (8)) reactions take place at the same equilibrium conditions as R1. In this way, the outlet gas composition from the co-electrolysis unit can be obtained.

The theoretical voltage of the co-electrolysis stack can be calculated based on the electrochemical equations pertaining to Nernst potential and polarization overpotentials (i.e., Ohmic, activation, and concentration overpotentials), which are listed in Table S4.

After obtaining the cell voltage, the required power for co-electrolysis can be further determined. The energy needed at given operating conditions for splitting steam and CO_2 to syngas can be derived from the following equations:

$$\Delta H = \Delta G + T\Delta S \quad (9)$$

$$V_{th} = \Delta H/2F \quad (10)$$

$$Q_{SOEC} = I(V_{th} - V_{cell}) \quad (11)$$

$$P_{SOEC} = IV_{cell} \quad (12)$$

where ΔH, ΔG, and $T\Delta S$ (Q) are the molar enthalpy, Gibbs energy, and entropy of the reaction, corresponding to total energy, electrical energy, and heat demand for the electrochemical reaction during co-electrolysis operation, respectively. V_{th} is the thermoneutral voltage (V), F is Faraday's constant (96485 C mol^{-1}), I is the electrical current (A), Q_{SOEC} and P_{SOEC} are heat and electric energy required (kW) for co-electrolysis at given working conditions, respectively. Notably, based on the heat balance of SOECs, when the cell voltage is above the thermoneutral voltage (i.e., $V_{cell} > V_{th}$), the cell is operated in exothermic mode, whereas when the cell voltage is below the thermoneutral voltage (i.e., $V_{cell} < V_{th}$), the cell is operated in endothermic mode.

To validate the co-electrolysis model, a number of experimental studies have been adopted for determining the key geometric parameters of the electrodes and electrolytes in the developed model. At first, the predicted values of outlet syngas composition from the co-electrolysis of steam and CO_2 process are compared with those obtained from the work of Cinti et al. (2016), where three various inlet gas conditions (i.e., S1, S2, and S3) were experimentally conducted. According to their cell material characteristic, as shown in Figs. S4 (a)-S4 (c), it is obvious that the present simulated results are well in line with the trend of experimental results. Next, the predictions of cell voltage along with current density are compared with different experimental measurements reported by Kazempoor and Braun (2014). This demonstrated good agreement between the predicted and the measured data (Fig. S4 (d)).

3.3. SOFC model and verification

Regarding the model of SOFC, as shown in Fig. S3, an integrated model of planar SOFCs with oxyfuel combustion for CO_2 capture has been developed and validated in this work. The detailed process flowsheet can be found elsewhere in the previous work (Kuo et al., 2021). However, coke oven gas (COG) and CO-rich gas obtained from the BF ironmaking process are adopted as fuel for the SOFCs. The pressurized gas stream is mixed with the anode-recycled gas at a steam-to-carbon ratio of 2.5 in order to avoid carbon deposition on the anode catalyst material. The following reactions at the anode side of the SOFC are taken into account, which is calculated based on the Gibbs free energy minimization method.

$$C_nH_m + nH_2O \leftrightarrow nCO + \left(n + \frac{m}{2}\right)H_2 \quad (13)$$

$$CO + H_2O \leftrightarrow CO_2 + H_2 \quad (14)$$

$$H_2 + 0.5O_2 \rightarrow H_2O \quad (15)$$

The cathode side of SOFC is modeled by a separator block, where the amount of oxygen transferred is determined by using a calculator block in Aspen Plus, and it depends on the fuel utilization factor. The calculated equations are defined as follows:

$$nO_{2,required} = 0.5(U_f)(nH_{2,equivalent}) \quad (16)$$

$$U_f = \frac{nH_{2,consumed}}{nH_{2,equivalent}} \quad (17)$$

$$nH_{2,\text{equivalent}} = nH_{2,in} + 1 \times n_{CO,in} + 4 \times n_{CH_4,in} \quad (18)$$

$$U_a = \frac{nO_{2,consumed}}{nO_{2,in}} \quad (19)$$

where $nO_{2,required}$ and $nO_{2,consumed}$ are the required and consumed amounts of oxygen at the anode and cathode (kmol h^{-1}), respectively. U_f is the fuel utilization factor, $nH_{2,consumed}$ and $nH_{2,equivalent}$ are consumed and equivalent amount of H_2 at the anode (kmol h^{-1}). U_a is the oxygen utilization factor and $nO_{2,in}$ is the amount of oxygen that passes through the cathode (kmol h^{-1}).

Subsequently, the anode-off gas is sent to a post-combustor via the oxyfuel combustion technology for the purpose of CO_2 capture. The high-purity oxygen is generated by an air separation unit (ASU), and it is utilized to combust the anode off-gas in an oxy-fuel combustor with 5 % in excess of the required quantity. The high-temperature flue gas primarily consists of CO_2 and steam, and it is partly recycled to the combustor to prevent too-high combustion temperatures. The concentrated CO_2 gas is finally obtained after entering the heat recovery steam generators (HRSG) and is used as another reactant for co-electrolysis.

The generated electric energy from SOFCs can be obtained at a certain operating current, which is expressed as:

$$I = \frac{(nH_{2,\text{equivalent}}) \times (2U_f F)}{3600} \tag{20}$$

$$P_{SOFC,AC} = P_{SOFC,DC} \times \eta_{inv} = I \times V_{cell} \times \eta_{inv} \tag{21}$$

where $P_{SOFC,AC}$ and $P_{SOFC,DC}$ are the AC and DC power output (kW), respectively. η_{inv} is the inverter efficiency (%), which is assumed to be 92 % (Atsonios et al., 2021).

The relevant electrochemical equations for the SOFC model are outlined in Table S5. It should be noted that the flowsheet in Aspen for both tubular and planar SOFCs is the same, although the geometric parameters of the cells differ (Kuo et al., 2021). To verify the accuracy of the developed planar SOFC, it has been further validated against experimental data, as shown in Fig. S5. The calculated cell voltage and overpotentials are in good agreement with those obtained from the experimental measurements.

3.4. Methanol synthesis model and verification

The methanol production routes from synthesis gas are modeled using a kinetic-based plug-flow reactor (PFR) in Aspen Plus. The reaction rate of syngas to methanol can be calculated using the Langmuir–Hinshelwood–Hougen–Watson (LHHW) rate expression and the reaction kinetic parameters based on the chemical reactions presented in Table S6.

$$CO + 2H_2 \leftrightarrow CH_3OH \tag{22}$$

$$CO_2 + 3H_2 \leftrightarrow CH_3OH + H_2O \tag{23}$$

$$CO_2 + H_2 \leftrightarrow CO + H_2O \tag{24}$$

$$r_{CH_3OH} = k_{CH_3OH} \frac{(p_{CO_2} p_{H_2}) - \left(\frac{1}{K_{pCH_3OH}}\right)\left(\frac{p_{CH_3OH} p_{H_2O}}{p_{H_2}^2}\right)}{\left(1 + K_a\left(\frac{p_{H_2O}}{p_{H_2}}\right) + K_b\sqrt{p_{H_2}} + K_c p_{H_2O}\right)^3} \tag{25}$$

$$r_{RWGS} = k_{RWGS} \frac{p_{CO_2} - \left(\frac{1}{K_{pRWGS}}\right)\left(\frac{p_{CO} p_{H_2O}}{p_{H_2}}\right)}{\left(1 + K_a\left(\frac{p_{H_2O}}{p_{H_2}}\right) + K_b\sqrt{p_{H_2}} + K_c p_{H_2O}\right)} \tag{26}$$

where r_i is the reaction rate (mol kg_{cat}^{-1} s^{-1}), k_i is the kinetic factor (kmol kg_{cat}^{-1} s^{-1} bar^{-1}), p_i is the partial pressure (bar), K_{pi} is the equilibrium constant (−), and K_a, K_b, and K_c are the adsorption constants (bar^n).

The Ergun equation is adopted to describe the pressure drop along the reactor length, which can be expressed as:

$$-\frac{dP}{dZ} = 150\frac{(1-\varepsilon)^2}{\varepsilon^3}\frac{\mu U}{\phi_s^2 D_p^2} + 1.75\frac{1-\varepsilon}{\varepsilon^3}\frac{\rho U^3}{\phi_s D_p} \tag{27}$$

where $\frac{dP}{dZ}$ is the change of pressure along the reactor length (Pa m^{-1}), ε is the void fraction (−), μ is the fluid viscosity (Pa s), U is the superficial velocity (m s^{-1}), ϕ_s is the particle shape factor (−), D_P is the particle diameter (m), and ρ is the fluid density (kg m^{-3}).

To check the accuracy of the kinetic model, it is validated against the literature data, as plotted in Fig. S6 in the Appendix. It shows that the established model gives reasonable results for methanol synthesis processes. Following the methanol production unit, the purification of crude methanol is carried out using a rigorous distillation column to produce high-quality methanol with a minimum of 99 wt% purity. On the other hand, the molar ratio of the reactant for the methanol synthesis reactor is controlled using a stoichiometric number ($SN = \frac{n_{H_2} - n_{CO_2}}{n_{CO} + n_{CO_2}}$) to equal to 2.04–2.05.

3.5. Vacuum Pressure Swing Adsorption (VPSA) CO_2 separation

In this study, the VPSA technology is selected to separate CO_2 from the BFG, which has already been proven to be a feasible approach for treating all the BFG. Meanwhile, an integrated top-gas recycling blast furnace with a VPSA plant was successfully demonstrated without main failures during the operation of the ULCOS project. The VPSA process is modeled according to the work of Arasto et al. (2014). The adsorption bed is operated at 3.5 bar, and the vacuum pressure at the outlet of the bed is 0.015 bar. The CO_2 stream is assumed to be separated at least 90 % purity, which is subsequently used as feedstock for co-electrolysis.

4. Performance analysis

Different process performance indicators of the four scenarios are compared in terms of energy conversion efficiency and environmental impact. It should be noted that the entire system analysis is evaluated based on the specific production rate in the BF (i.e., 1000 kg of hot metal).

4.1. Energy analysis

The energy conversion efficiency (η_{En}) of the integrated BF-SOCs-methanol process is defined as follows:

$$\eta_{En}\,(\%) = \frac{\dot{m}_{CH_3OH} \cdot LHV_{CH_3OH}}{\dot{m}_{BFG} \cdot LHV_{BFG} + \dot{m}_{COG} \cdot LHV_{COG} + Q_{process} + W_{SOEC} + W_{net}} \times 100 \tag{28}$$

$$W_{net} = W_{SOFC} + W_{HRSG} - W_{VPSA} - W_{ASU} - W_{AUX} \tag{29}$$

where $\dot{m}_{CH_3OH}$ is the mass flow rate of methanol in the outlet of the system (kg h^{-1}); $\dot{m}_{BFG}$ and $\dot{m}_{COG}$ are the mass flow rate of BFG and COG in the inlet of the system (kg h^{-1}), respectively; LHV_{CH_3OH} is the lower heating values of methanol products (kJ kg^{-1}), and LHV_{BFG} and LHV_{COG} are the lower heating value of BFG and COG (kJ kg^{-1}), respectively. $Q_{process}$ and W_{net} are the required heat and net power within the integrated BF-SOCs-methanol process (kW), respectively. The gross power output from the process is contributed by SOFC and heat recovery steam generator (HRSG), whereas the power consumption is the sum of VPSA, air separation unit (ASU), and auxiliary units. Notably, the specific power consumption of 0.269 kWh kg^{-1} is adopted for pure O_2 production in the ASU (Esfilar et al., 2018).

Apart from energy conversion efficiency, another important indicator for evaluating carbon utilization merit can be carbon conversion efficiency, representing the ratio of the amount of recycled carbon being converted into methanol to the total amount of carbon fed into the system:

$$\textit{Carbon conversion efficiency}\,(\%) = \frac{\dot{m}_{CH_3OH}}{\dot{m}_{CO} + \dot{m}_{CO_2}} \times 100 \tag{30}$$

4.2. Carbon emissions analysis

To evaluate the reduction potential of CO_2 via the proposed integrated BF-SOCs-methanol process, various environmental performance indicators are taken into account. The system boundary for carbon emission assessment is shown in Fig. 3.

The carbon intensity of methanol production from the entire process is calculated by the following equations (Qiu et al., 2023):

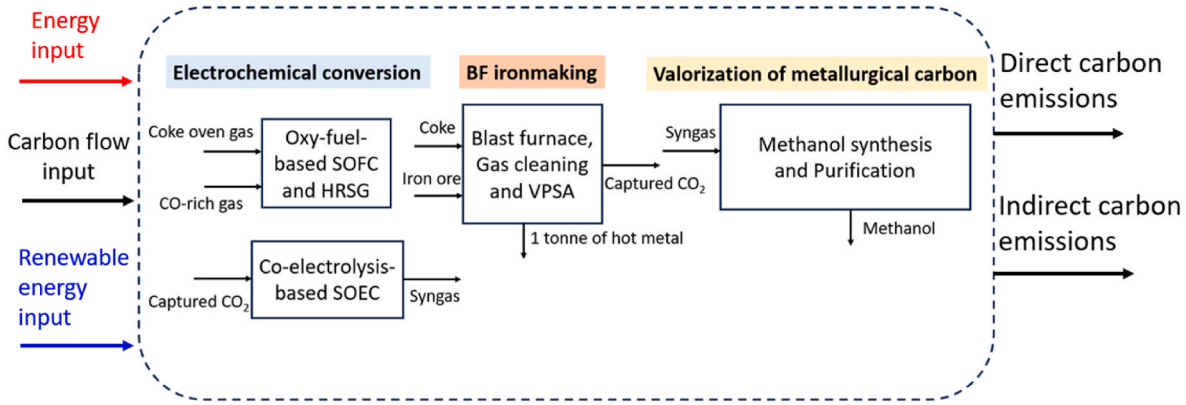

Fig. 3. System boundary for carbon emissions evaluation.

$$Carbon\ intensity\ (kg-CO_2/kg-methanol)=\frac{CO_2\ emission\ balance}{\dot{m}_{CH_3OH}} \tag{31}$$

$$CO_2\ emission\ balance\ (kg\,h^{-1})=Total\ CO_2\ emission-Total\ CO_2\ feed \tag{32}$$

$$Total\ CO_2\ emission\ (kg\,h^{-1})=CO_{2Flue\ gas}+CO_{2utilities}+CO_{2thermal}-CO_2\ feed \tag{33}$$

$$Total\ CO_2\ feed\ (kg\,h^{-1})=CO_2\ from\ BFG+CO_2\ from\ COG \tag{34}$$

Notably, total CO_2 emission is the sum of direct CO_2 emission from the process (i.e., VPSA and methanol synthesis) and indirect CO_2 emission contributed by the use of electrical and thermal energy. Regarding the indirect CO_2 emission, it is assumed that CO_2 intensities of electricity and heat are 205.3 lb-CO_2 MMBtu^{-1} (0.3177 kg kW^{-1} h^{-1}) and 0.655 kg CO_2 kW^{-1} h^{-1}, respectively (Qiu et al., 2023; Ramirez et al., 2019). In contrast, the total CO_2 feed represents the total amount of BFG and COG fed into the SOCs and methanol synthesis processes, which is based on per ton of hot metal production from the BF.

As a result, the reduction potential of CO_2 between the conventional blast furnace ironmaking process (i.e., all the generated BFG and COG are combusted) and the new process can be determined by:

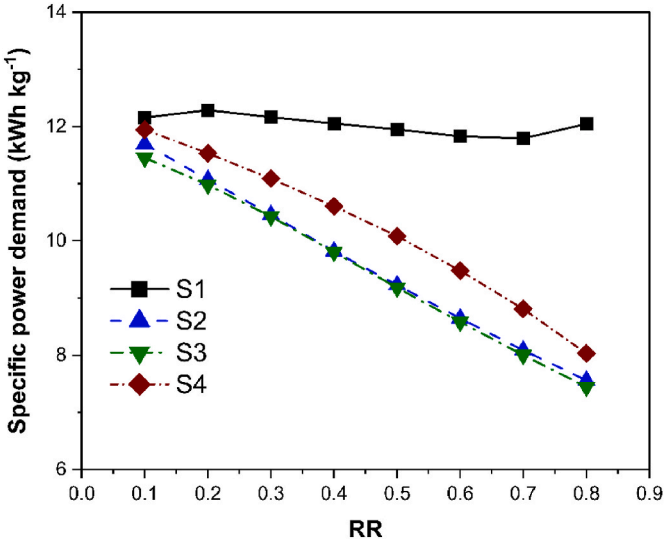

Fig. 4. Influence of the RR on the specific power demand of methanol production.

$$CO_2\ reduction\ potential\ (\%)=\frac{CO_2\ emission_{conventional}-CO_2\ emission_{new}}{CO_2\ emission_{conventional}}\times 100 \tag{35}$$

5. Results and discussion

The influence of RR on the subsystem performance of the four scenarios is first discussed. Apart from S4, where the operating conditions for the recirculation loop within the co-electrolysis unit are fixed, opting a higher RR leads to a decrease in the concentrations of CO_2 and H_2O and an increase in those of CO and H_2 in the inlet stream of the co-electrolysis unit. It should be noted that this higher RR demands more renewable power to drive the electrochemical reactions. As mentioned earlier, to prevent the oxidation of cathode, 10 % of H_2 in the inlet stream of the co-electrolysis unit is typically needed. To achieve this threshold, the RRs of S1, S2, and S4 (i.e., short-loop recirculation) should be controlled to around 0.2, whereas that of S3 (i.e., long-loop recirculation) should be adjusted to at least around 0.4. Fig. 4 shows that for S1, S2, S3, and S4 as the RR is varied from 0.1 to 0.8, the specific power demand of methanol production varied in the range between 12.16 and 12.05 kWh kg^{-1}, 11.70–7.56 kWh kg^{-1}, 11.45–7.44 kWh kg^{-1}, and 11.94–8.03 kWh kg^{-1}. The lower values of specific power demand of methanol production obtained for S2 and S3 can be mainly attributed to higher methanol yields through the long-loop recirculation scheme.

Fig. 5 reveals the distribution of methanol production rate (Fig. 5a) and carbon conversion efficiency (Fig. 5b) within the investigated range of RR. The methanol production rate of the four scenarios is in the range of 13.26–16.96 kmol h^{-1} for S1, 14.57–24.06 kmol h^{-1} for S2, 13.82–23.78 kmol h^{-1} for S3, and 14.11–21.00 kmol h^{-1} for S4. Overall, the methanol production rate can be significantly increased by 28–72 % with the increase of RR. Moreover, by using the recirculation design, S2 and S3 can generate relatively much more methanol than that of S1 and S4. This can be attributed to the fact that the unconverted carbon sources from the methanol synthesis unit are further recycled back to the co-electrolysis unit, which helps to enhance the methanol yield. Contrary to S1 and S4, the recirculation loop is only erected in a short loop (i.e., co-electrolysis alone or methanol synthesis alone), resulting in more carbon emission to the environment (Fig. 9 for additional explanations).

As far as carbon conversion efficiency is concerned, as shown in Fig. 5b, the range of its values are 40.57–51.91 %, 44.58–73.63 %, 42.29–72.77 %. and 43.17–64.27 %, corresponding to S1, S2, S3, and S4, respectively. It is clear that S2 and S3 offer higher carbon conversion throughout the process due to a long recirculation configuration.

The overall system performance analysis in terms of energy

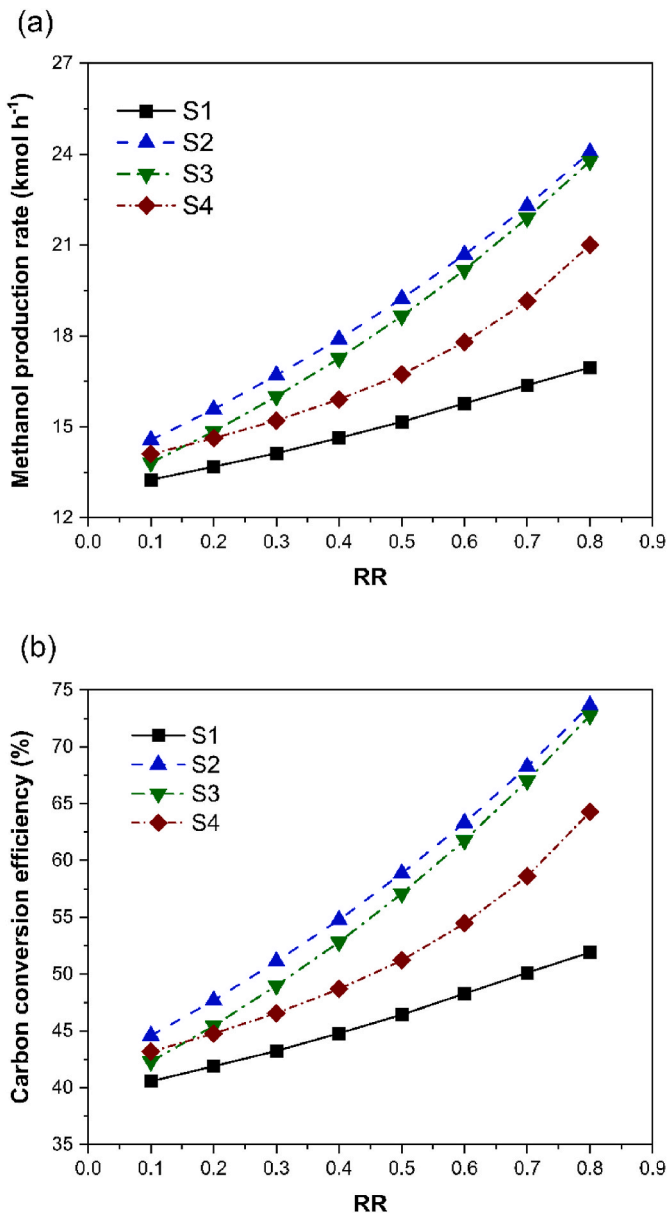

Fig. 5. Influence of the RR on the (a) methanol production rate and (b) carbon conversion efficiency.

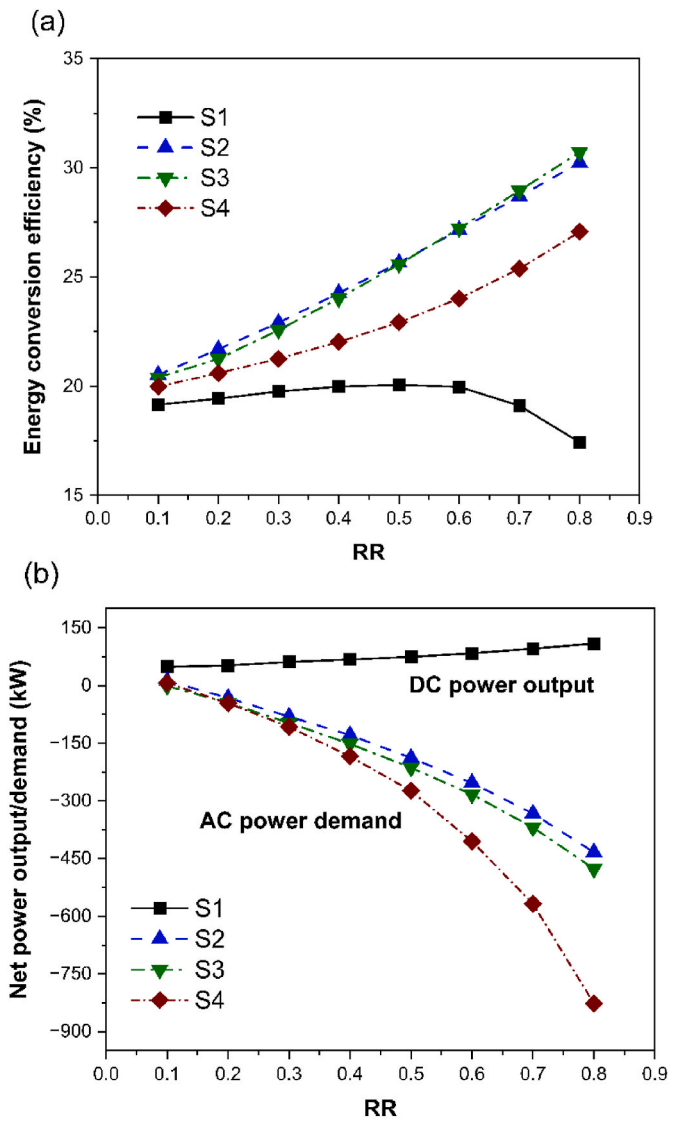

Fig. 6. Influence of the RR on the (a) energy conversion efficiency and (b) net power output.

conversion efficiency and carbon emissions for the four different plant schemes are shown in Figs. 6–10. Fig. 6a displays a comparison of plant conversion efficiency with regard to various process configurations. The highest energy conversion efficiency of the plant of 30.72 % at RR = 0.8 is achieved for S3, followed by 30.23 % at RR 0.8 for S2, 27.07 % at RR 0.8 for S4, and 20.06 % at RR 0.5 for S1. For S2, S3, and S4, the energy conversion efficiency increased almost linearly as a function of RR. However, it is worth noting that, for S1, the optimal operating value of RR is 0.5, after which an apparent decreasing trend can be found. The main reason for this trend could be attributed to a large amount of process heat required for pre-heating both the anode and cathode inlet of the co-electrolysis system. This can be seen in Fig. 8a, which depicts the process heat demand as a function of RR.

The energy output from the plant includes thermal energy output of methanol product and net power generation. The former ranges between 2348.19 and 3004.25 kW for S1, 2580.09–4261.71 kW for S2, 2447.96–4211.83 kW for S3, and 2498.5–3720.1 kW for S4. The variation of thermal energy output is proportional to the methanol production rate. As mentioned earlier, S2 and S3 can yield higher methanol production rates, thus leading to higher thermal energy output. The latter for the four scenarios is shown in Fig. 6b, where it can be seen that aside from S1, the net power output is negative, meaning that the total power output from the SOFCs and the HRSG put together is not sufficient to cover the required auxiliary power due to energy-intensive syngas compression under high RR operation (Fig. 7).

The breakdown of each component for power consumption is illustrated in Fig. 7. Notably, in each process scheme, the total power output is unchanged at a constant value of 1002.31 kW (AC) because of the constant flowrate of input fuel (i.e., based on per ton of hot metal produced) for SOFCs fed by COG and CO-rich gas. Notably, the power consumption for balance of the plant in the SOFCs process has been taken into account in the net power output. Hence, 89.01 % of electric power output (AC) is contributed by SOFCs, while that of 10.99 % is obtained by the HRSG process. Regarding the breakdown of total power consumption, it can be seen that the energy required for CO_2 capture from the BFG (VPSA) is constant, regardless of the process configuration. On examining the power consumption of the syngas compressor, with an increase of RR, the increased volumetric flow of recirculated gas causes larger power requirements for S2, S3, and S4. Nevertheless, unlike them, no recirculation loop is established for S1, thus showing the opposite

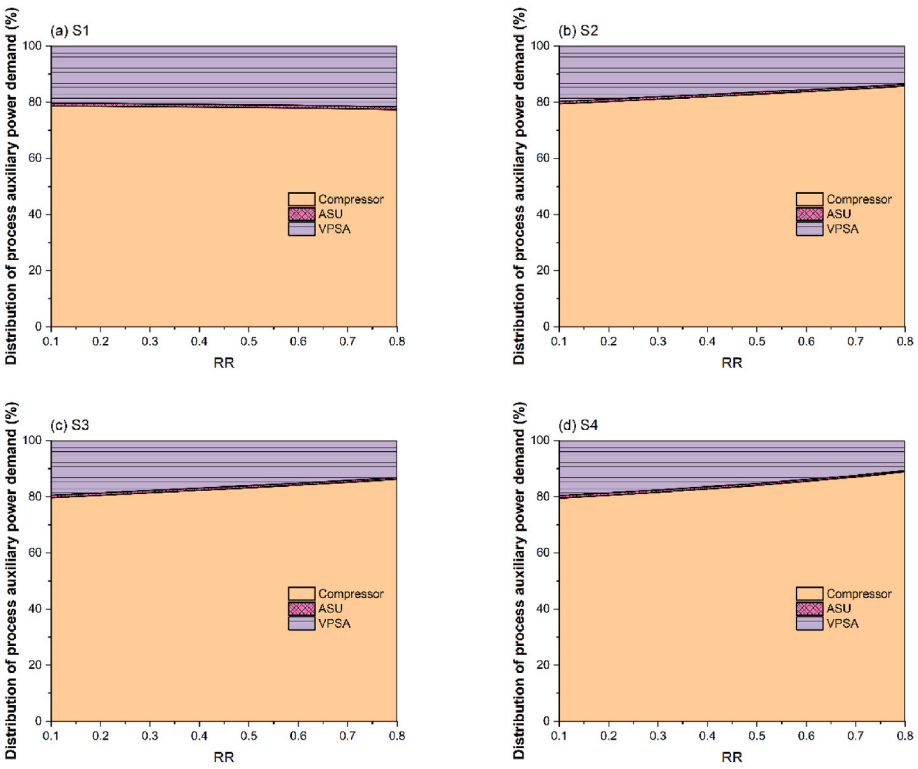

Fig. 7. Breakdown of auxiliary power consumption as a function of the RR: (a) S1, (b) S2, (c) S3, and (d) S4.

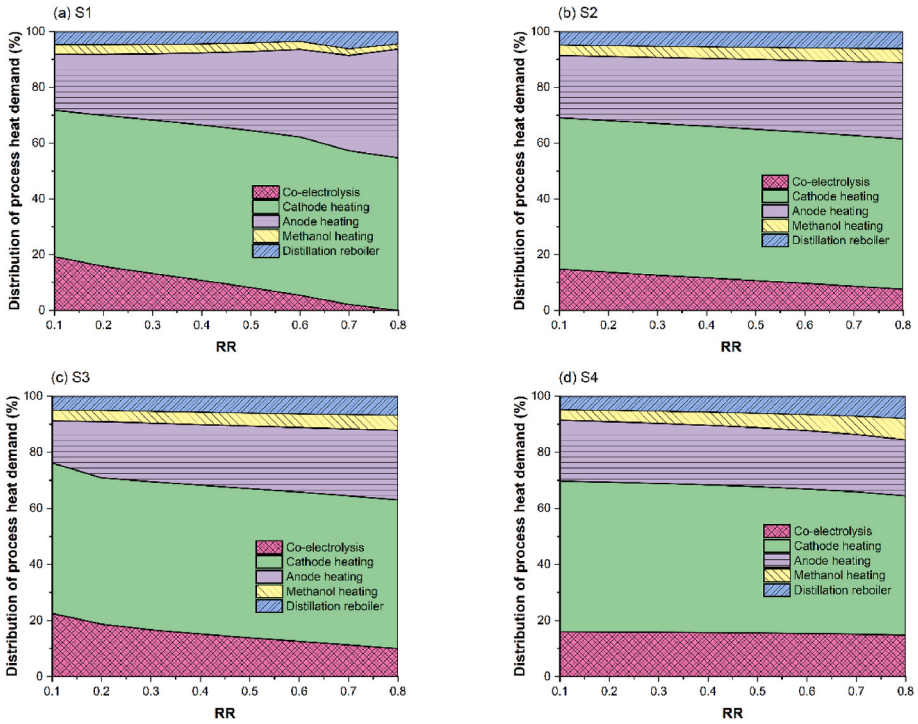

Fig. 8. Breakdown of process heat demand as a function of the RR, for various configurations: (a) S1, (b) S2, (c) S3, and (d) S4.

trend with the RR.

Fig. 8 depicts a breakdown of the demand for process heat, which can be classified into the heat demand for SOEC, the balance of the plant, and the heat demand for methanol synthesis and purification. In the case of co-electrolysis, heat is required during operation in endothermic mode. The balance of the plant accounts for the heat demand needed for water evaporation, as well as for the inlet reactants and air on the cathode and anode sides, respectively. In the case of methanol synthesis, the amount of heat is necessary to reach the desired operating temperature of the methanol reactor and subsequent purification through distillation. It should be noted that the thermal energy requirement for heating components is first evaluated by adopting electrical heaters

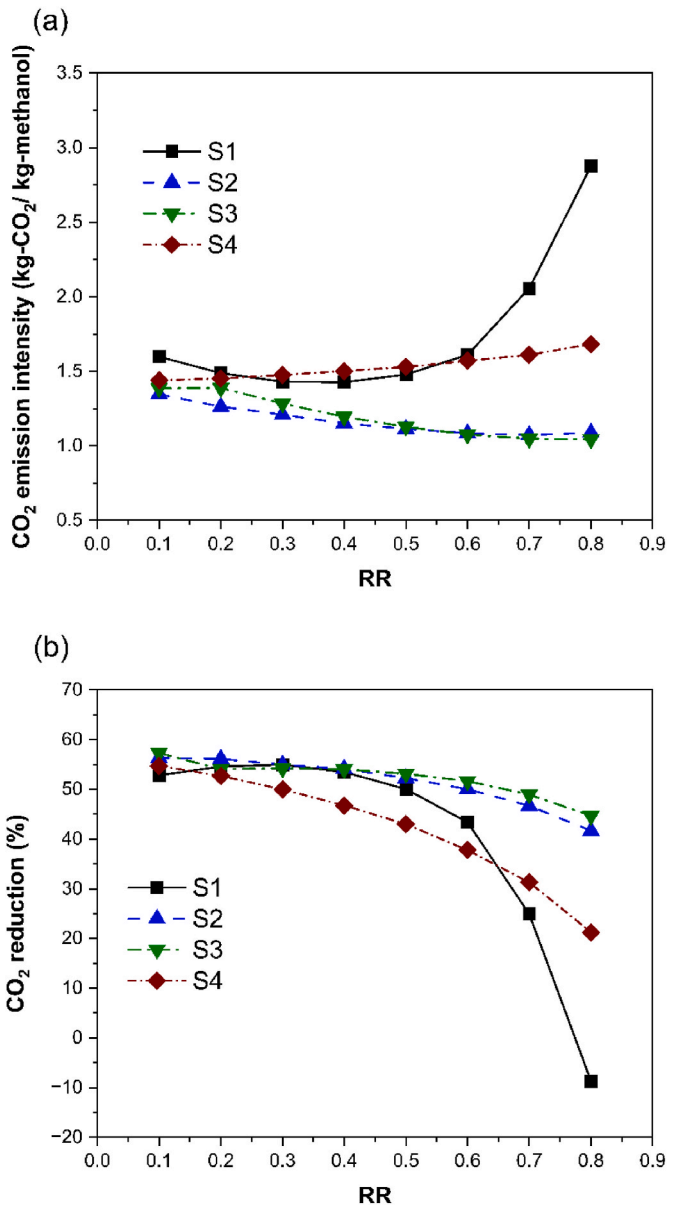

Fig. 9. Influence of the RR on the (a) carbon emission intensity and (b) CO_2 reduction potential.

prior to performing heat-integration design.

Except for S4, for which RR was kept constant, the heat demand for co-electrolysis in S1, S2, and S3 decreased with rising RR owing to the higher current density used. However, the heat demand for the balance of the plant increased because of the enlarged amount of recirculated gas. For S2, S3, and S4, more recirculated gas must be reheated in an electrical heater before being fed into the methanol synthesis reactor. This leads to a more significant amount of heat (i.e., methanol heating) being supplied from the external heat source. In contrast, the opposite trend can be found in S1 due to the lack of a recycle loop in the methanol synthesis process. Thus, it can be concluded that for S2, S3, and S4, the energy consumption of the plant is primarily contributed by both process heat demand and renewable power required for the co-electrolysis unit.

Fig. 9 illustrates the effect of RR on carbon emission intensity (Fig. 9a) and carbon reduction potential (Fig. 9b) for four various configurations. As a whole, similar trends in carbon emission intensity are observed, showing a minimum value, regardless of the configuration considered. The minimum values are 1.43, 1.07, 1.05, and 1.44 kg-CO_2/kg-methanol at RRs of 0.4, 0.7, 0.7. and 0.1, respectively, corresponding to S1, S2, S3, and S4. It is evident that the carbon emission intensity of S2 and S3 is substantially reduced by approximately 25–27 % compared to S1 and S4 under the above operating conditions.

A breakdown of the carbon emission sources from the plant is shown in Fig. 10. This indicates that, except for S1, the highest amount of carbon emissions is attributed to thermal energy-related sources, followed by auxiliary power-related sources, and direct carbon emissions from the plant.

Moreover, it should be noted that, as shown in Fig. 10, except for S1, the total carbon emissions from auxiliary power increase dramatically with increasing RR. The primary reason for this is that when the RR exceeds 0.2, the power output generated by the SOFC and HRSG is insufficient to meet the plant's auxiliary power requirements. In particular, more auxiliary power is required for the syngas compressor in S4 compared to S2 and S3, leading to significantly higher indirect carbon emissions. On the other hand, S2 exhibits the lowest direct carbon emissions in flue gas (117.85 kg-CO_2/h), followed by S3 (132.56 kg-CO_2/h), S1 (221.22 kg-CO_2/h), and S4 (255.95 kg-CO_2/h) at a RR of 0.8.

The carbon reduction potential (Fig. 9b) based on the net carbon balance (Eqs. (31)–(35)) varies between 21.25 % and 57.30 % compared to the direct combustion of BFG and COG (i.e., 1438.11 kg-CO_2/h) in the conventional BF ironmaking system. Among the four process schemes, S2 and S3 are more environmentally attractive than S1 and S4, regardless of the RR adopted. The maximum carbon saving is 57.30 % for S3 and 56.31 % for S2, both occurring at a RR value of 0.1. In all cases, it is also revealed that a higher RR results in a lower carbon reduction potential due to the significant demand for thermal energy and parasitic power when the RR exceeds 0.4.

To sum up, comparing the previous merits in terms of energy conversion efficiency and environmental impact assessment, it can be concluded that a trade-off between these two key process performance indicators should be simultaneously considered while determining the optimal operating window of RR for each case. In addition, the risk of carbon deposition on the cathode of the co-electrolysis unit and piping could be explicitly increased under high RR operation. Based on the above considerations, the following heat-integration design selects a RR where the carbon reduction potential can reach approximately 50 %. As a result, the RRs of 0.5, 0.6, 0.7, and 0.3, corresponding to S1, S2, S3, and S4, respectively, are taken into account for the heat-integration configurations to enhance the process efficiency further and reduce the carbon emission intensity. On the other hand, the impact of the operating pressure of the methanol synthesis reactor on the various key performance indicators are also examined in Fig. S7. Obviously, higher pressure operation is beneficial to methanol production rate, thereby enhancing the energy conversion efficiency and lowering the CO_2 emission intensity. However, it can be observed that the improvement of both process performance indicators is limited once the operating pressure is higher than 70 bar because of the increased electricity demand. Considering the economic viability, the operating pressure of 70 bar is used for the thermal integration analysis. Meanwhile, according to the ternary C-H-O diagram under thermodynamic equilibrium, as shown in Fig. S8, the risk of carbon deposition on the fuel electrode of the co-electrolysis cell could be prevented under these conditions for all scenarios.

Based on the pinch analysis (Fig. S9), the maximum possible heat recovery between hot and cold fluids, as well as the minimum demand for utilities within the process, can be determined. The pinch point of the integrated plant for all scenarios is located at 35 °C following a minimum temperature difference of 10 °C between hot and cold streams. Table 3 shows the heat-integration results for four different process configurations. About 1910–3627 kW of heating duty and 3203–3639 kW of cooling duty can be recovered after thermal integration of the process, accounting for 59.22–75.36 % and 85.99–88.75 % reduction in energy demand for process heating and cooling, respectively.

A comparison of process performance before and after thermal

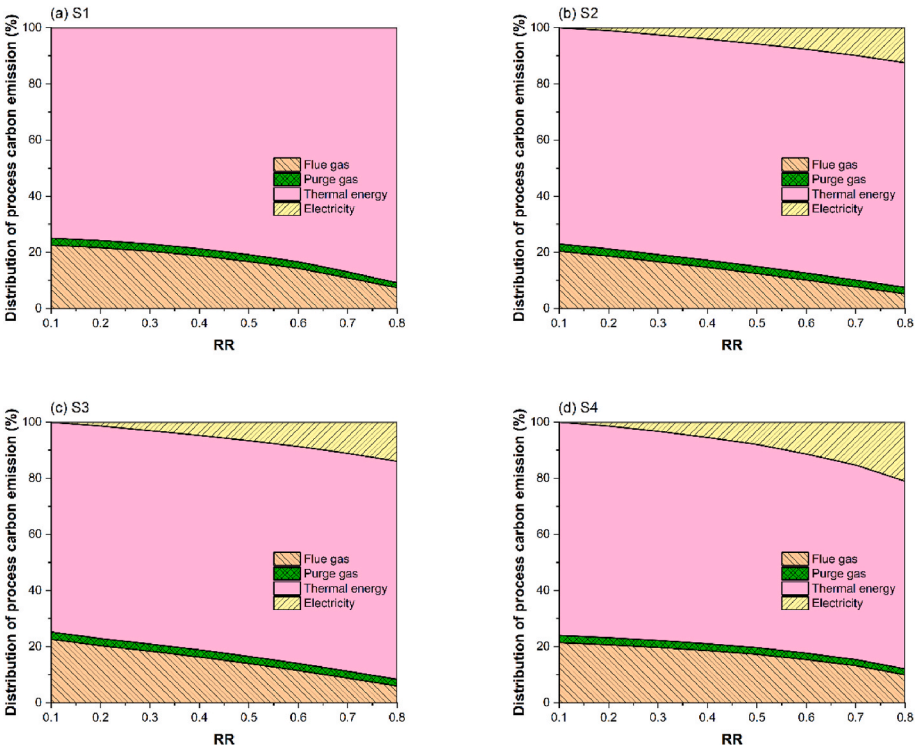

Fig. 10. Breakdown of process carbon emission as a function of the RR: (a) S1, (b) S2, (c) S3, and (d) S4.

Table 3
Heat-integration results for four different process configurations.

Scenarios		Utilities	
		Heating duty (kW)	Cooling duty (kW)
S1 (RR = 0.5)	Before HI	4812.59	4100.39
	After HI	1185.84	461.45
S2 (RR = 0.6)	Before HI	4566.91	3871.92
	After HI	1148.34	443.47
S3 (RR = 0.7)	Before HI	4361.05	3655.12
	After HI	1159.94	452.27
S4 (RR = 0.3)	Before HI	3225.07	3986.72
	After HI	1315.32	558.58

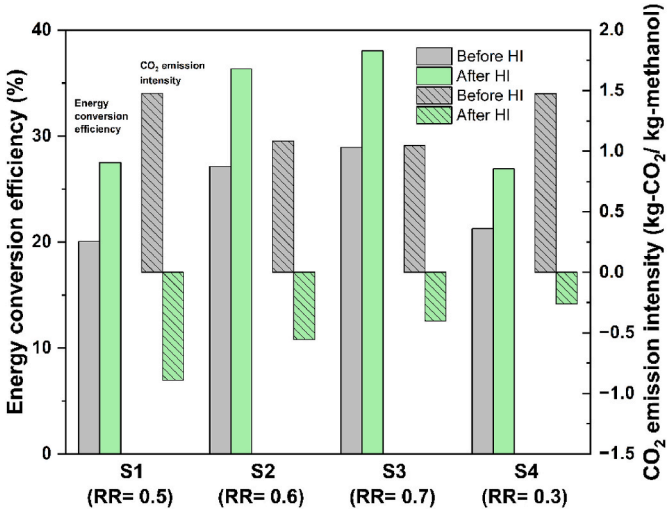

Fig. 11. Process performances before and after heat integration for all scenarios.

integration of the four scenarios under their suggested RRs is displayed in Fig. 11. Based on two key performance merits, compared to the process without thermal integration, the energy conversion efficiency enhanced by 5.66–9.20 %, while net negative CO_2 emissions is achievable based on the evaluated system boundary (Fig. 3), regardless of the scenario. As shown in Table S7, this is mainly due to the significant reduction in thermal energy requirements (Fig. 10), resulting in a substantial decrease in CO_2 emissions related to indirect carbon emissions. Moreover, both S1 and S4 have energy conversion efficiency lower than 30 %, even though S1 can emit the least CO_2 emissions. In contrast, both S2 and S3 offer relatively high energy conversion efficiency of 36.35 % and 38.05 %, demonstrating promising pathways for efficient CO_2 reduction in the blast furnace ironmaking process through renewable energy sources utilization.

6. Conclusions

An innovative electrochemical conversion process for the valorization of metallurgical exhaust gases, namely, BFG and COG, into methanol is proposed. The first-of-its-kind integrated model, which consists of a blast furnace with co-electrolysis, oxyfuel-based SOFC, and methanol synthesis units, was successfully developed in Aspen Plus. Various process configurations of tail gas recirculation for enhancing the conversion efficiency of methanol and reducing the environmental impact of the BF ironmaking process were evaluated. The main conclusions inferred are:

(1) With the tail gas recirculation design, the methanol production rate can be significantly enhanced by around 28–72 %. Long-loop recirculation design (S2 and S3) yields a higher methanol production rate than that of short-loop one (S1 and S4).
(2) The achievable carbon conversion efficiency of the proposed plant could range from 41 % to 73 %. Among the four process configurations, the long-loop recirculation configuration can offer higher carbon conversion efficiency.

(3) The highest energy conversion efficiency is found to be 31 % (S3), 30 % (S2), 27 % (S4), and 20 % (S1), corresponding to RRs of 0.8, 0.8, 0.8, and 0.5, respectively.
(4) The majority of energy demand for the integrated BF-SOC-methanol synthesis plant could be attributed to the thermal energy and renewable energy needed for the co-electrolysis unit. In particular, SOFC and HRSG's power generation is insufficient to compensate for the energy-intensive syngas compression at higher RR operation.
(5) As for environmental impact assessment, the minimum carbon emission intensity of methanol is around 1.43 kg-CO_2/kg-methanol for S1, 1.07 kg-CO_2/kg-methanol for S2, 1.05 kg-CO_2/kg-methanol for S3, and 1.44 kg-CO_2/kg-methanol for S4, corresponding to RR values of 0.4, 0.7, 0.7, and 0.1, respectively. Notably, lower carbon emission intensity for S2 and S3 can be achieved compared to S1 and S4. The main contribution to carbon emission intensity could be due to a significant amount of process heat demand, followed by power consumption, and direct carbon emissions.
(6) Based on the net carbon balance, the carbon emissions for the proposed plant could be dramatically reduced by around 21–57 % before the heat-integration design, especially for S2 and S3. However, higher RRs lead to lower carbon reduction potential due to higher indirect carbon emission associated with thermal energy and auxiliary power.
(7) With the heat integration design, an additional 5.66–9.20 % of energy conversion efficiency enhancement is obtained, thereby demonstrating the maximum energy conversion efficiency of 36 % for S2 and 38 % for S3. It turns out that carbon-negative methanol production processes are achievable, regardless of the process configuration considered, based on the evaluated system boundary.

CRediT authorship contribution statement

Po-Chih Kuo: Writing – review & editing, Writing – original draft, Project administration, Investigation, Conceptualization. **Faruk Özdemir:** Writing – review & editing, Validation, Software, Investigation. **Yin-Ping Wu:** Software, Investigation. **Biju Illathukandy:** Writing – review & editing, Writing – original draft, Validation, Investigation. **Wei Wu:** Writing – review & editing, Validation, Resources, Project administration, Conceptualization. **Muhammad Aziz:** Writing – review & editing, Validation, Resources, Project administration, Conceptualization.

Declaration of competing interest

The authors declare that they have no known competing financial interests or personal relationships that could have appeared to influence the work reported in this paper.

Acknowledgments

The authors acknowledge the financial support of the Japan Society for the Promotion of Science (JSPS) under grant number JP-22F21041 and JSPS KAKENHI grant number JP24K01415, National Science and Technology Council, Taiwan under grant 112-2622-8-006-020 and 113-2321-B-029-002, as well as Ministry of National Education, Turkey.

Appendix A. Supplementary data

Supplementary data to this article can be found online at https://doi.org/10.1016/j.jclepro.2025.146853.

Data availability

Data will be made available on request.

References

Arasto, A., Tsupari, E., Kärki, J., Lilja, J., Sihvonen, M., 2014. Oxygen blast furnace with CO_2 capture and storage at an integrated steel mill-Part I: technical concept analysis. Int. J. Greenh. Gas Control 30, 140–147.
Ariyama, T., Sato, M., 2006. Optimization of ironmaking process for reducing CO_2 emissions in the integrated steel works. ISIJ Int. 46, 1736–1744.
Artz, J., Müller, T.E., Thenert, K., Kleinekorte, J., Meys, R., Sternberg, A., Bardow, A., Leitner, W., 2018. Sustainable conversion of carbon dioxide: an integrated review of catalysis and life cycle assessment. Chem. Rev. 118 (2), 434–504.
Ateka, A., Rodriguez-Vega, P., Ereña, J., Aguayo, A.T., Bilbao, J., 2022. A review on the valorization of CO_2. Focusing on the thermodynamics and catalyst design studies of the direct synthesis of dimethyl ether. Fuel Process. Technol. 233, 107310.
Atsonios, K., Samlis, C., Manou, K., Nikolopoulos, A., Sfetsioris, K., Mitsotakis, A., Grammelis, P., 2021. Technical assessment of LNG based polygeneration systems for non-interconnected island cases using SOFC. Int. J. Hydrogen Energy 46, 4827–4843.
Bailera, M., 2023. Comparing different syngas for blast furnace ironmaking by using the extended operating line methodology. Fuel 333, 126533.
Bailera, M., Lisbona, P., Peña, B., Romeo, L.M., 2021. A review on CO_2 mitigation in the iron and steel industry through power to X processes. J. CO2 Util. 46, 101456.
Bampaou, M., Haag, S., Kyriakides, A.-S., Panopoulos, K.D., Seferlis, P., 2023. Optimizing methanol synthesis combining steelworks off-gases and renewable hydrogen. Renew. Sustain. Energy Rev. 171, 113035.
Bampaou, M., Panopoulos, K., Seferlis, P., Sasiain, A., Haag, S., Wolf-Zoellner, P., Lehner, M., Rog, L., Rompalski, P., Kolb, S., Kieberger, N., Dettori, S., Matino, I., Colla, V., 2022. Economic evaluation of renewable hydrogen integration into steelworks for the production of methanol and methane. Energies 15, 4650.
Cinti, G., Discepoli, G., Bidini, G., Lanzini, A., Santarelli, M., 2016. Co-electrolysis of water and CO_2 in a solid oxide electrolyzer (SOE) stack. Int. J. Energy Res. 40, 125–284.
Collis, J., Duch, K., Schomäcker, R., 2022. Techno-economic assessment of jet fuel production using the Fischer-Tropsch process from steel mill gas. Front. Energy Res. 10.
Collis, J., Strunge, T., Steubing, B., Zimmermann, A., Schomäcker, R., 2021. Deriving economic potential and GHG emissions of steel mill gas for chemical industry. Front. Energy Res. 9.
Deng, L., Adams II, T.A., 2020. Techno-economic analysis of coke oven gas and blast furnace gas to methanol process with carbon dioxide capture and utilization. Energy Convers. Manag. 204, 112315.
Dipu, A.L., Ujisawa, Y., Ryu, J., Kato, Y., 2014. Carbon dioxide reduction in a tubular solid oxide electrolysis cell for a carbon recycling energy system. Nucl. Eng. Des. 271, 30–35.
Esfilar, R., Mehrpooya, M., Moosavian, S.M.A., 2018. Thermodynamic assessment of an integrated biomass and coal cogasification, cryogenic air separation unit with power generation cycles based on LNG vaporization. Energy Convers. Manag. 157, 438–451.
Flores-Granobles, M., Saeys, M., 2020. Minimizing CO_2 emissions with renewable energy: a comparative study of emerging technologies in the steel industry. Energy Environ. Sci. 13, 1923–1932.
Gentile, G., Bonalumi, D., Pieterse, J.A.Z., Sebastiani, F., Lucking, L., Manzolini, G., 2022. Techno-economic assessment of the FReSMe technology for CO_2 emissions mitigation and methanol production from steel plants. J. CO2 Util. 56, 101852.
Girod, K., 2020. Methanol synthesis with steel-mill gases: simulation and practical testing of selected gas utilization scenarios. Processes 8, 1673.
Hauser, A., Wolf-Zoellner, P., Haag, S., Dettori, S., Tang, X., Mighani, M., Matino, I., Mocci, C., Colla, V., Kolb, S., Bampaou, M., Panopoulos, K., Kieberger, N., Rechberger, K., Karl, J., 2022. Valorizing steelworks gases by coupling novel methane and methanol synthesis reactors with an economic hybrid model predictive controller. Metals 12, 1023.
Holappa, L., 2020. A general vision for reduction of energy consumption and CO_2 emissions from the steel industry. Metals 10, 1117.
Hu, Y., Rufford, T.E., Chen, J., Hao, L., Li, M., Qiu, Y., Garg, S., Rudolph, V., Wang, G., 2023. Opportunities to reduce energy consumption and CO_2 emissions from ironmaking blast furnace using CO_2 electrolysis to CO for carbon recycling. J. Clean. Prod. 389, 135997.
Kazempoor, P., Braun, R.J., 2014. Model validation and performance analysis of regenerative solid oxide cells for energy storage applications: reversible operation. Int. J. Hydrogen Energy 39, 5955–5971.
Kim, D., Han, J., 2020. Techno-economic and climate impact analysis of carbon utilization process for methanol production from blast furnace gas over Cu/ZnO/Al_2O_3 catalyst. Energy 198, 117355.
Kong, R., Zhang, R., Li, H., Wu, Y., Sun, Z., Sun, Z., 2022. A new pathway to produce hydrogen with CO_x capture from blast furnace gas via SOFC-SOEC integration. Energy Convers. Manag. 271, 116278.
Kuo, P.C., Illathukandy, B., Kung, C.H., Chang, J.S., Wu, W., 2021. Process simulation development of a clean waste-to-energy conversion power plant: thermodynamic and environmental assessment. J. Clean. Prod. 154, 488–501.

Lundgren, J., Ekbom, T., Hulteberg, C., Larsson, M., Grip, C.-E., Nilsson, L., Tunå, P., 2013. Methanol production from steel-work off-gases and biomass based synthesis gas. Appl. Energy 112, 431–439.
Lipiäinen, S., Sillman, J., Vakkilainen, E., Soukka, R., Tuomaala, M., 2024. Hydrogen transport options for a large industrial user: analysis on costs, efficiency, and GHG emissions in steel mills. Sustain. Prod. Consum. 44, 1–13.
Marocco, P., Gandiglio, M., Audisio, D., Santarelli, M., 2023. Assessment of the role of hydrogen to produce high-temperature heat in the steel industry. J. Clean. Prod. 388 (15), 135969.
Porter, R.T.J., Cobden, P.D., Mahgerefteh, H., 2022. Novel process design and techno-economic simulation of methanol synthesis from blast furnace gas in an integrated steelworks CCUS system. J. CO2 Util. 66, 102278.
Qian, Y., Li, Y., Hao, Y., Yu, T., Hu, H., 2024. Greenhouse gas control in steel manufacturing: inventory, assurance, and strategic reduction review. Carbon Res. 3, 27.
Qiu, F., Sun, Z., Li, H., Qian, Q., 2023. Process simulation and multi-aspect analysis of methanol production through blast furnace gas and landfill gas. Energy 285, 128609.
Ramirez, A.D., Rivela, B., Boero, A., Melendres, A.M., 2019. Lights and shadows of the environmental impacts of fossil-based electricity generation technologies: a contribution based on the Ecuadorian experience. Energy Policy 125, 467–477.
Safarian, S., 2023. To what extent could biochar replace coal and coke in steel industries? Fuel 339, 12740.
Schittkowski, J., Ruland, H., Laudenschleger, D., Girod, K., Kähler, K., Kaluza, S., Muhler, M., Schlögl, R., 2018. Methanol synthesis from steel mill exhaust gases: challenges for the industrial Cu/ZnO/Al_2O_3 catalyst. Chem. Ing. Tech. 90, 1419–1429.
Schittkowski, J., Zeidler-Fandrich, B., Müller, T., Schlögl, R., Ruland, H., 2022. The Carbon2Chem® laboratory in Oberhausen -A workplace for lab-scale setups within the cross-industrial project. Chem. Ing. Tech. 94, 1397–1404.
Suzuki, K., Hayashi, K., Kuribara, K., Nakagaki, T., Kasahara, S., 2015. Quantitative evaluation of CO_2 emission reduction of active carbon recycling energy system for ironmaking by modeling with aspen plus. ISIJ Int. 55, 340–347.
Uribe-Soto, W., Portha, J.F., Commenge, J.M., Falk, L., 2017. A review of thermochemical processes and technologies to use steelworks off-gases. Renew. Sustain. Energy Rev. 74, 809–823.
Voß, J.M., Daun, T., Geitner, C., Schluter, S., Schulzke, T., 2022. Operating behavior of a demonstration plant for methanol synthesis. Chem. Ing. Tech. 94, 1489–1500.
World Steel Association https://worldsteel.org (access on 2025 July).
Xu, Y.P., Liu, R.H., Shen, M.Z., Lv, Z.A., Chupradit, S., Metwally, A.S.M., Sillanpaa, M., Qian, Q., 2022. Assessment of methanol and electricity co-production plants based on coke oven gas and blast furnace gas utilization. Sustain. Prod. Consum. 32, 318–329.
Yang, Y., Li, G., Luo, T., Pan, J., Song, Y., Qian, Q., 2023. Multi-aspect comparative analyses of two innovative methanol and power cogeneration systems from two different sources. Int. J. Hydrogen Energy 48, 1120–1135.
Yildirim, Ö., Nölker, K., Büker, K., Kleinschmidt, R., 2018. Chemical conversion of steel mill gases to urea: an analysis of plant capacity. Chem. Ing. Tech. 90, 1529–1535.
Yilmaz, C., Wendelstorf, J., Turek, T., 2017. Modeling and simulation of hydrogen injection into a blast furnace to reduce carbon dioxide emissions. J. Clean. Prod. 154, 488–501.